Self-Sensing Actuation for Piezoelectric and MEMS Devices in Data Storage Applications

Chee Khiang Pang[1], Fan Hong[2], Wai Ee Wong[2], and Tong Heng Lee[1]

***Abstract*—Currently, position sensors other than the Read/Write (R/W) heads are not embedded in Hard Disk Drives (HDDs) due to cost, resolution, and Signal-to-Noise (SNR) issues. In MEMS-actuated platforms, a row of capacitive comb drives is commonly dedicated as actuator while the other opposite row as sensor, thereby reducing effective force and actuation. In this paper, we apply Self-Sensing Actuation (SSA) to piezoelectric elements in the PZT active suspension for commercial dual-stage HDDs. The developed methodology is extended to Capacitive SSA (CSSA) for MEMS micro X-Y stage in Probe-Based Storage Systems (PBSSs). The proposed Indirect-Driven SSA (IDSSA) and CSSA schemes yield high SNR and nanometer resolution experimental measurements comparable to those from the Laser Doppler Vibrometer (LDV), which are crucial for advanced servo systems in the next generation of ultra-high density data storage devices.**

***Index Terms*—MEMS, Probe-Based Storage Systems (PBSSs), Self-Sensing Actuation (SSA).**

I. Introduction

Currently in 2010, many consumer portable electronics such as digital cameras, video recorders, and cell phones, *etc.*, carry vast amount of data and hence require ultra-high density data storage devices of smaller sizes and form factors. To keep up with the insatiable consumers' demands in today's information explosion era, data storage companies have proposed to enhance current magnetic HDDs with dual-stage technologies by appending a secondary actuator onto the primary actuator Voice Coil Motor (VCM), or the futuristic Micro-Electrical-Mechanical-Systems (MEMS)-actuated Probe-Based Storage Systems (PBSSs) as showcased in the "Millipede" [1].

As such, it is important to save sensor costs and increase Signal-to-Noise Ratio (SNR) of measurement of states, while improving sensor-actuator collocation for next generation of data storage devices. On appending extraneous sensors for active control in HDDs, rotational accelerometers are used to damp the VCM butterfly mode in a single-stage HDD [2]. The authors in [3] split the two PZT strips in a PZT-actuated suspension and use one strip of PZT element as actuator and the other as sensor for active vibration control in a dual-stage HDD. [4] uses the PZT elements in the entire compound actuator solely as a position sensor. For PBSSs, external non-intrusive thermal sensors are also used for absolute position sensing of the cantilever tips in the "Millipede" [1].

In this paper, the SSA (Self-Sensing Actuation) methodology by employing the PZT elements in the PZT active suspension in dual-stage HDDs as a secondary actuator and displacement sensor *simultaneously* [5] is enhanced and extended to an Indirect-Driven SSA (IDSSA) methodology and applied onto a commercial dual-stage HDD. The SSA methodology is also extended to capacitive comb drives in MEMS-actuated devices, and a Capacitive SSA (CSSA) circuit is proposed for using the comb drives in the MEMS micro X-Y stage as sensors and actuators simultaneously as well [6].

II. Self-Sensing Actuation (SSA)

When piezoelectric materials (*e.g.* PZT elements) are subjected to strain, charges arise on the surface of the material and hence set up an electric field which allows piezoelectric materials to be used as actuators and sensors simultaneously, or commonly known as SSA. SSA is attractive in active control applications because the actuator and sensor arrangement is a near-collocated pair, thereby avoiding non-minimum phase zero dynamics and spillover which degrades tracking performance.

A. Indirect-Driven SSA (IDSSA) Bridge Circuit

For the PZT active suspension, the PZT elements are modelled as a capacitor C_p in series with a dependent voltage source v_p, with C_p representing the dipoles while v_p representing the electric field setup by the dipoles during actuation. C_p can be measured via a balanced AC bridge circuit *a prior*. Furthering our earlier works in [5], we propose an enhanced SSA circuit in the so-called Indirect-Driven SSA (IDSSA) as shown in Fig. 1. Unlike in [5] where the PZT active suspension is driven by the *same* control voltage v_{in} *directly*, the proposed IDSSA bridge circuit uses the high gain property of the operational amplifiers (*i.e.*, $V_+ \approx V_-$) to drive the PZT active suspension *indirectly* from the other input terminal of the operational amplifier. When the IDSSA bridge circuit in Fig. 1 is subjected to control voltage v_{in}, the PZT active suspension is actuated and displaced, thereby generating voltage v_p which arises from mechanical strain. The following relationships hold.

$$v_1 = \frac{1+2\pi f R_2(C_2+C_p)}{1+2\pi f R_2 C_2} v_{in} - \frac{2\pi f R_2 C_p}{1+2\pi f R_2 C_2} v_p \quad (1)$$

$$v_2 = \frac{1+2\pi f R_1(C_1+C_p')}{1+2\pi f R_1 C_1} v_{in} \quad (2)$$

This work was supported in part by Singapore MOE AcRF Tier 1 Grant R-263-000-564-133.

[1]C. K. Pang and T. H. Lee are with Department of Electrical and Computer Engineering, National University of Singapore, Republic of Singapore.

[2]W. E. Wong and F. Hong are with A*STAR Data Storage Institute, Republic of Singapore.

Corresponding author: Chee Khiang Pang, Department of Electrical and Computer Engineering, National University of Singapore, 4 Engineering Drive 3, Singapore 117576. Email: justinpang@nus.edu.sg

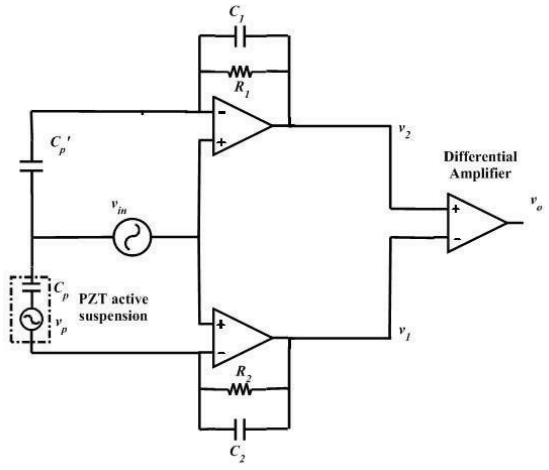

Fig. 1. Proposed Indirect-Driven SSA (IDSSA) bridge circuit employing the PZT active suspension as a secondary actuator and sensor simultaneously. The PZT elements are modelled as a capacitor C_p with dependent voltage source v_p.

$$\begin{aligned} v_o &= v_2 - v_1 \\ &= \left[\frac{1+2\pi f R_1(C_1+C_p')}{1+2\pi f R_1 C_1} - \frac{1+2\pi f R_2(C_2+C_p)}{1+2\pi f R_2 C_2}\right] v_{in} \\ &\quad + \frac{2\pi f R_2 C_p}{1+2\pi f R_2 C_2} v_p \end{aligned} \tag{3}$$

If $C_1 = C_2 = C_p' = C_p$ and $R_1 = R_2$, the bridge circuit is said to be *balanced* and we can obtain

$$v_o = \frac{2\pi f R_1 C_p}{1+2\pi f R_1 C_p} v_p. \tag{4}$$

As such, v_p is decoupled from the control signal v_{in} and can be used for feedback control. When applied to commercial dual-stage HDDs, the proposed IDSSA requires only additional cheap electronic circuitry and does not reduce the effective stroke of the PZT active suspension. The only trade-off is the requirement of a larger control signal v_{in} for the same amount of displacement actuation, as compared to that without the IDSSA bridge circuit. We can now decouple the variable voltage v_p (hence strain/displacement information) using the IDSSA bridge circuit in Fig. 1 for SNR and correlation studies.

B. SNR and Correlation

Let v_{LDV} be the voltage obtained from the non-intrusive displacement measurements using the Laser Doppler Vibrometer (LDV). Firstly, we capture the frequency response of $\frac{v_{\text{LDV}}(s)}{v_o(s)}$ or our experiments by injecting v_{LDV} into Channel 1 and the IDSSA bridge circuit's output v_o into Channel 2 of the Dynamic Signal Analyzer (DSA). The frequency responses were collected with three swept sine excitation signals of amplitudes of v_{in} at 300 mV, 400 mV, and 500 mV. The measured and modelled frequency responses were plotted in Fig. 2.

To compare the estimated displacement of the PZT active suspension and that measured by the LDV, the modelled

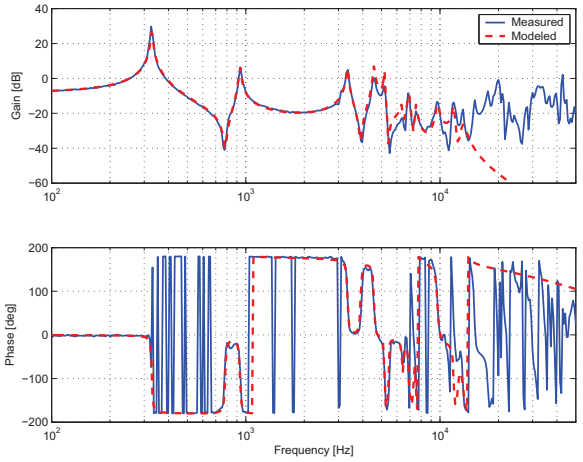

Fig. 2. Frequency response of $\frac{v_{\text{LDV}}(s)}{v_o(s)}$.

transfer function shown in Fig. 2 was discretized at a sampling rate of 100 kHz and implemented on the dSPACE real-time system. v_o is channelled into $\frac{v_{\text{LDV}}(z)}{v_o(z)}$, and its output is the estimated displacement of the PZT active suspension $\hat{v}_{\text{LDV}}$. Similarly by injecting v_{LDV} into Channel 1 and $\hat{v}_{\text{LDV}}$ into Channel 2 of the DSA, we obtain the frequency response of $\frac{v_{\text{LDV}}(z)}{\hat{v}_{\text{LDV}}(z)}$ as shown in Fig. 3.

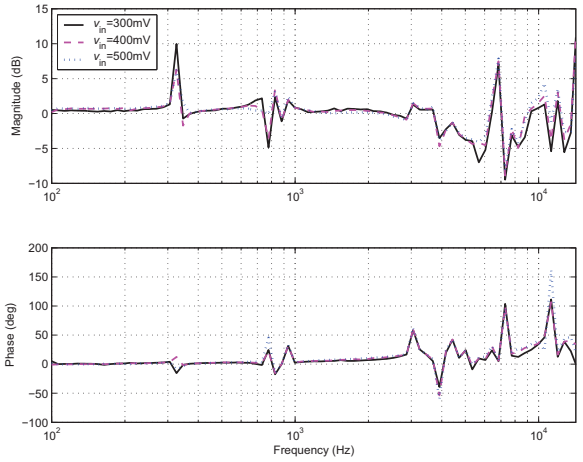

Fig. 3. Frequency response of $\frac{v_{\text{LDV}}(z)}{\hat{v}_{\text{LDV}}(z)}$.

Ideally, this frequency response should be of unity gain (0 dB) with a phase loss, identical to that of a delay term. However, it can be seen that the estimated displacement output $\hat{v}_{\text{LDV}}$ gives a good agreement with the actual displacement measured from LDV v_{LDV} from 100 Hz to 10 kHz, and the discrepancy at higher frequency range is due to the unmodelled dynamics which can be seen in Fig. 2.

In addition, the time measurements of the actual displacement v_{LDV} and estimated displacement output $\hat{v}_{\text{LDV}}$ using a sinusoid of $0.126 \sin 2\pi 2000t$ V are shown in Fig. 4. It can be seen that our proposed IDSSA circuit gives a higher SNR estimation, and is not corrupted with a low frequency signal

caused by the environmental disturbance. The smallest input voltage given is 126 mV, and this corresponds to a 2 nm displacement of the PZT active suspension at the R/W head. The IDSSA bridge circuit can detect nanoposition measurements with higher SNR as compared to that from the LDV.

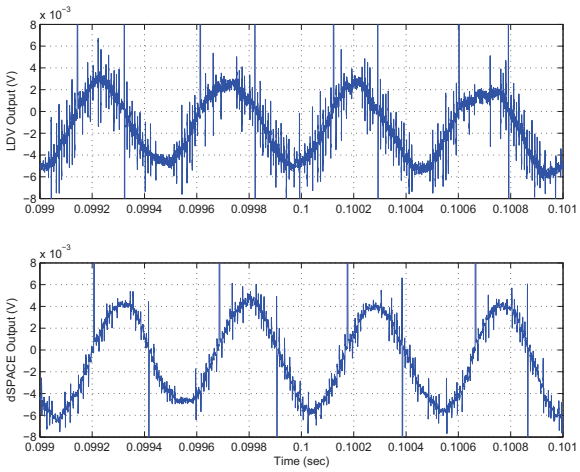

Fig. 4. Comparison of displacements. Top: measured from LDV. Bottom: estimated from proposed IDSSA bridge circuit.

III. Capacitive Self-Sensing Actuation (CSSA)

Many universities and research institutes are working on PBSSs. While their approaches may differ, the main components used for high speed parallel Read/Write/Erase (R/W/E) data are similar. A PBSS in the so-called "Nanodrive" is shown in Fig. 5. In this section, we extend the concept of SSA to Capacitive SSA (CSSA) for the fabricated MEMS micro X-Y stage in the "Nanodrive".

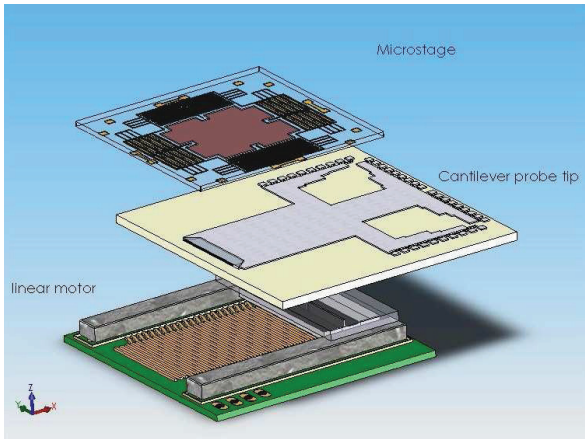

Fig. 5. Components of proposed PBSS in the so-called "Nanodrive" consisting of (i) cantilevers carrying probe tips (ii) linear motor and (iii) MEMS micro X-Y stage with recording medium.

The details of the comb drives and the suspensions for the fabricated MEMS micro X-Y stage are shown in Fig. 6. The finger width is 4 μm and the gap is 3 μm. The length of the finger is 75 μm, and the overlap of each pair of fingers is 30 μm.

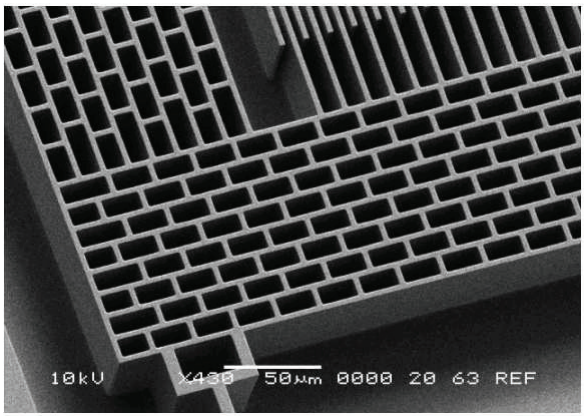

Fig. 6. Details of comb drives in the MEMS micro X-Y stage used in the "Nanodrive" under SEM. Plan view of the fingers (top right).

As the actuation of the MEMS micro X-Y stage is in the in-plane direction, non-intrusive online measurements of axial displacements and velocities are not possible even upon release of the MEMS micro X-Y stage from the wafer. As such, offline measurements from high speed cameras coupled with image processing techniques are commonly used for frequency response measurements. We propose the CSSA scheme shown in Fig. 7 to detect the position of the MEMS micro X-Y stage *in situ*. This is in contrast to the "Millipede" where thermal sensors are used to detect the absolute position of the heated cantilever tips [1].

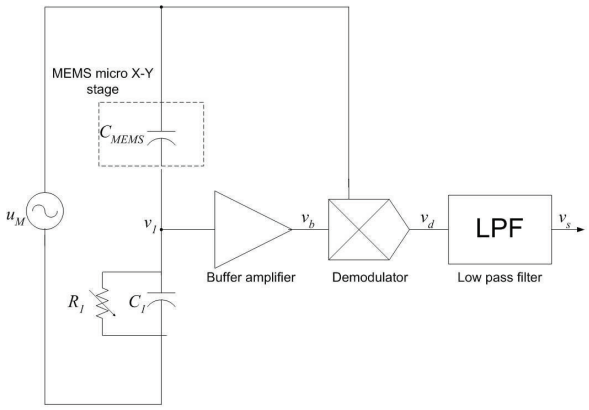

Fig. 7. CSSA bridge circuit employing the MEMS comb drives as an actuator and sensor simultaneously. The MEMS devices are modelled as a capacitor C_{MEMS}.

Using the fact that the capacitance C_{MEMS} of the comb drives in the MEMS micro X-Y stage is proportional to the area of overlap A, we have

$$C_{\text{MEMS}} = \frac{\varepsilon_r \varepsilon_o A}{d}, \tag{5}$$

which is in turn proportional to displacement of the MEMS micro X-Y stage for the same comb width. Now, the CSSA

bridge circuit in Fig. 7 is constructed to achieve actuation and sensor capabilities simultaneously, similar to SSA in piezoelectric actuators [5]. This allows us to decouple the capacitance information C_{MEMS} from input signal u_M, and is directly proportional to displacement of the MEMS micro X-Y stage.

In Fig. 7, assume that the signal generator u_M produces a sinusoid $U \sin \omega t$ of angular frequency ω rad/s. As such, the following equations hold

$$v_1 = \frac{C_{\text{MEMS}}}{C_1 + C_{\text{MEMS}}} U \sin \omega t \quad (6)$$

$$v_b = K_a v_1 \quad (7)$$

$$v_d = v_b u_M = K_a v_1 U \sin \omega t = \frac{U^2 K_a C_{\text{MEMS}}}{C_{\text{MEMS}} + C_1} \sin^2 \omega t$$

$$= \frac{U^2 K_a C_{\text{MEMS}}}{2(C_{\text{MEMS}} + C_1)} (1 - \cos 2\omega t), \quad (8)$$

where K_a is the gain of the buffer amplifier. After filtering with the Low Pass Filter (LPF), the high frequency sinusoid at 2ω is demodulated and v_s can be obtained as

$$v_s = \frac{U^2 K_a C_{\text{MEMS}}}{2(C_{\text{MEMS}} + C_1)}, \quad (9)$$

and hence we can interpolate C_{MEMS} to be

$$C_{\text{MEMS}} = -\frac{2 v_s C_1}{2 v_s - U^2 K_a} \quad (10)$$

which is proportional to the area of overlap A (hence displacement) of the MEMS micro X-Y stage in both axial directions. The above derivations exclude the effects of resistor R_1, which is commonly included to prevent drifting effects of the capacitance after prolonged operations.

The capacitance of MEMS-based devices are usually in the pico- or even femto-Farad region. When actuated in micro- or even nanometers, the SNR is very low. As such, the modulator and demodulator in Fig. 7 are added to reduce the sensor noise level and improve SNR. An external sinusoidal modulator signal is also essential to achieve high SNR capacitive sensing, and is used to actuate the MEMS micro X-Y stage for obtaining position information through artificially vibrating the MEMS micro X-Y stage at a frequency ω during calibration of the proposed CSSA circuit. It should be noted that a sinusoid of frequency higher than the closed-loop bandwidth of the MEMS micro X-Y stage should be used during R/W/E operations after calibration, to prevent vibration and excitation of the stage.

For our experiments, capacitors in the pico-Farad range as well as a sinusoidal modulator signal of 5 kHz are used. The demodulator, an LPF of corner frequency at 10 kHz, and the interpolator in (10) are implemented on a dSPACE DS1103 board at a sampling frequency of 400 kHz. The experimental results of proposed CSSA showing linearity of output DC voltage v_{DC} and change in capacitance ΔC are shown in Fig. 8 [6]. An identified linear relationship of

$$v_{\text{DC}} = -0.07 \Delta C - 0.11 \quad (11)$$

is obtained.

It can be seen from Fig. 8 that the output DC voltage is linear with change in capacitance ΔC which is in turn, is proportional to displacement of the MEMS micro X-Y stage. The proposed CSSA scheme calibrated with the measurements from the high speed cameras can then be used for absolute displacement sensing in both axial X and Y directions.

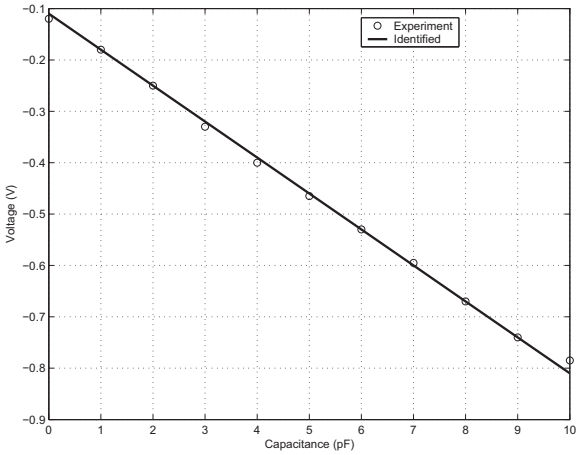

Fig. 8. Experimental results of proposed CSSA.

IV. Conclusion

In this paper, we apply Self-Sensing Actuation (SSA) to construct a cheap and collocated PZT active suspension's displacement sensor with nanoposition resolution. The proposed Indirect Driven Self-Sensing Actuation (IDSSA) bridge circuit estimates the PZT active suspension's displacement with high correlation and SNR, without compromising its effective stroke in a commercial dual-stage Hard Disk Drive (HDD). The SSA methodology is extended to a Capacitive SSA (CSSA) scheme for sensor fusion in MEMS devices and Probe-Based Storage Systems (PBSSs). Our experimental results of both SSA and CSSA show their feasibilities in achieving self-sensing and collocated sensor fusion, with the required SNR for next generation of ultra-high density enhanced dual-stage HDDs or PBSSs.

References

[1] E. Eleftheriou, T. Antonakopoulos, G. K. Binning, G. Cherubini, M. Despont, A. Dholakia, U. Dürig, M. A. Lantz, H. Pozidis, H. E. Rothuizen, and P. Vettiger, "Millipede–A MEMS-Based Scanning-Probe Data-Storage System," *IEEE Trans. Magn.*, Vol. 39, No. 2, pp. 938–945, March 2003.

[2] F. Y. Huang, W. Imaino, F. Lee, and T. Semba, "Active Damping in HDD actuator," *IEEE Trans. Magn.*, Vol. 37, No. 2, pp. 847–849, March 2001.

[3] Y. Li, R. Horowitz, and R. Evans, "Vibration Control of a PZT Actuated Suspension Dual-Stage Servo System Using a PZT Sensor," *IEEE Trans. Magn.*, Vol. 39, No. 2, pp. 932–937, 2003.

[4] S. -H. Lee, C. C. Chung, and C. W. Lee, "Active High-Frequency Vibration Rejection in Hard Disk Drives," *IEEE/ASME Trans. Mechatron.*, Vol. 11, No. 3, pp. 339–345, June 2006.

[5] C. K. Pang, G. Guo, B. M. Chen, and T. H. Lee, "Self-Sensing Actuation for Nanopositioning and Active-Mode Damping in Dual-Stage HDDs," *IEEE/ASME Trans. Mechatron.*, Vol. 11, No. 3, pp. 328–338, June 2006.

[6] C. K. Pang, Y. Lu, C. Li, J. Chen, H. Zhu, J. Yang, J. Mou, G. Guo, B. M. Chen, and T. H. Lee, "Design, Fabrication, Sensor Fusion, and Control of a Micro X-Y Stage Media Platform for Probe-Based Storage Systems," *Mechatronics*, Vol. 19, No. 7, pp. 1158–1168, October 2009.